JMEPEG (2008) 17:506–516
DOI: 10.1007/s11665-007-9183-3

1059-9495/$19.00

The Corrosion Effects on the Structural Integrity of Reinforcing Steel

Ch. Alk. Apostolopoulos, D. Michalopoulos, and P. Koutsoukos

(Submitted September 7, 2007; in revised form November 19, 2007)

An experimental study conducted on 12 mm diameter, artificially corroded BSt500$_s$ steel rebars, showed that the mass loss, the fatigue limit, and the life expectancy were reduced according to the level of corrosion. Rebar corrosion has a great impact on the mass loss, mechanical properties, low cycle fatigue (LCF) and there is strong indication that embrittlement takes place. The extended salt-spray exposure enhanced the damage and promoted extended creation of pits and perforations suggesting progressive embrittlement and reduction of the available energy, justified by the SEM micrograph results. The low cycle strain-controlled fatigue testing under ±1, ±2.5, and ±4% constant amplitude strain indicated that the corroded steel bars exhibit gradual reduction in available energy, number of cycles to failure, and load bearing ability. For the ±1% strain level the fatigue limit was reduced considerably as the level of corrosion increased due to mass loss and reduction of the exterior martensitic layer. In addition, a drastic drop in the energy density of the specimens was observed with creation of stress concentration points. At ±2.5% and ±4% strain levels, the fatigue limit was reduced dramatically mainly due to accumulated damage from plastic deformation and minimally due to corrosion. Anti-seismic design that ignores the influence of corrosion and cumulative damage due to plastic deformation, and the mechanical behavior of reinforcing steel during severe ground motion, could lead to unpredictable performance.

Keywords BSt500$_s$ steel rebars, corrosion, embrittlement, fatigue, mass loss

1. Introduction

Steel rebar corrosion appears to be the main reason for structural concrete degradation, it constitutes a serious problem in seismic areas and is a serious safety and economic issue. Repetitive stresses cause fatigue damage to materials which is considered to be an inevitable and irreversible process. The high pH level of the concrete pore solution, provides protection to the reinforcing steel, by forming a thin oxide passive layer covering the reinforcement. This layer remains stable in the alkaline concrete environment of pΘ 12.5-13, but begins to deteriorate when the pH of the pore solution drops below 11 (Ref 1, 2). The corrosion rate rises when the pH drops under 9. For corrosion to commence, the oxide film must be broken or depassivated, which may occur if the alkalinity of the pore water in the concrete pores decreases and/or penetration of the chloride ions takes place. This may be caused by carbonation, especially in the proximity of cracks, or by water dilution, which accompanies cracking (Ref 3, 4). The advancing corrosion results in reduction of the load carrying cross section of the bars and increases their volume by 3 to 8 times, which in turn causes the buildup of internal stresses with eventual cracking and spalling of the concrete cover. This leads to corrosion escalation (Ref 5, 6). Usually the layer of corrosion products consists of water and hydrated iron oxides, which due to their volumetric expansion develop cracks in the concrete leaving the reinforcing steel unprotected to corrosion (Ref 7). Corrosion cracks are usually parallel to the reinforcement, and are thus quite distinct from transverse cracks associated with tension in the reinforcement caused by loading. As the corrosion proceeds, the longitudinal cracks widen and, together with structural transverse cracks, may cause concrete spalling. Even though steel corrosion affects concrete durability, no relationship between corrosion level and load carrying capacity of structural members has been established yet. Steel corrosion and associated cracking and spalling of concrete have been identified as the most severe forms of deterioration. At rebar corrosion of about 7% and 12% the rib profile loss is around 45% and 70% accordingly, which explains the steel bar slippage mode of failure (Ref 8-10). The climatic conditions in locations near the sea, constitute one of the most aggressive environments for concrete structures due to the high ambient salinity, temperature, and humidity, and also due to the ingress of chlorine through wind borne salt. Chloride induced damage of reinforcing steel results in concrete cracking and spalling, destruction of the protective steel barrier and formation of pits, notches and cavities on the steel surface. The chlorides within the salt act as a catalyst in the natural corrosion process. Once corrosion commences, the reinforcement is eventually replaced by rust, a porous product of higher volume than the steel which exerts tensile forces on the surrounding concrete thus inducing delamination along the interface between steel and concrete (Ref 11).

Ch. Alk. Apostolopoulos and **D. Michalopoulos**, Department of Mechanical Engineering and Aeronautics, University of Patras, Patras 26500, Greece; and **P. Koutsoukos**, FORTH-ICEHT and Department of Chemical Engineering, University of Patras, P.O. Box 1414, Patras 26504, Greece. Contact e-mail: charrisa@mech.upatras.gr.

Strain-controlled LCF is considered to be a method of testing steel under cyclic varying loading. The results derived under LCF are utilized in order to estimate the remaining life of steel that may also contain cracks, notches, holes, ribs, fillets, and other discontinuities, and which in many instances are due to corrosion, material flaws or poor design. Correlation of the life expectancy of materials to fatigue strength and damage parameters, such as stress, strain, plastic, and strain energy density, have been investigated in the past. Since fatigue damage and dissipation of strain energy during each loading cycle are inter-related and due to the irreversibility of the microplastic deformation, the life expectancy can be correlated to plastic and strain energy. The strain energy dissipated during each cycle may be regarded as fatigue damage. Therefore, the fatigue life has been represented by the cyclic plastic strain energy measured from the hysteresis loop. In the HCF regime, where the material behaves elastically and the fatigue life is significantly influenced by the mean stresses, the plastic energy cannot be used as a damage parameter (Ref 12). Seismic loads act on the load-bearing elements of structures in the form of high strain reversals, simulated as single axis low cycle fatigue (Ref 13). The Fourier spectra of ground movement during an earthquake that occurred in Japan showed that the loading was cyclic and the frequency corresponding to the maximum amplitude was approximately 2 Hz (Ref 14). Investigation of the catastrophic earthquake of Tang Shan in China confirmed that the failure mode of the building structural steel was LCF (Ref 13). During seismic movement, structures are subjected to alternating shear forces and bending moments. This cyclic motion results in the gradual bursting and detachment of the concrete cover, which finally leaves the reinforcing steel bars as the sole load-bearing elements thus forcing them to carry both the shear forces and the bending moments, leading to permanent plastic deformation of the steel, while the compressive concrete zone is destroyed (Ref 15).

The reduction in the structural performance of reinforced concrete members due to corroded steel is caused by the loss in the effective cross-sectional area of concrete due to cracking in the cover concrete, loss in the mechanical properties and performance of reinforcing bars due to reduction of their cross-sectional area. It has been attempted to quantify corrosion and mass loss of steel with the reduction of its mechanical properties. Even though the impact of corrosion on the strength of steel reinforcing bars is well known, the current design codes do not face the problem since they are unable to quantify it and need further review (Ref 16-22). Rebar corrosion is of paramount importance in seismic areas, since during strong earthquake activity, the requirement for structures with high ductility is necessary. Steel corrosion, combined with tensile and compressive stresses, the predisposition of the material for fracture, the level of corrosive atmosphere, and the size of the implied mechanical stresses eventually leads to fracture (Ref 23). The result of such a combination may be the fast degradation and failure of the material. Corrosion fracture combined with mechanical loading is accelerated also due to localized pitting and cracking.

In the present study, the integrity of corroded $BSt500_s$ steel rebars is investigated under LCF. The results were correlated with the loss of the exterior martensitic layer and the damage observed in SEM micrographs on transverse and longitudinal sections.

2. Experimental Procedure and Discussion of Results

2.1 Induced Corrosion

$BSt500_s$ ribbed steel rebars 12 mm in diameter were artificially corroded in a specially designed salt-spray corrosion chamber, according to ASTM B117-94 standard, for 10, 20, 30, 45, 60, and 90 days. To accelerate corrosion, the specimens were sprayed in a 5% sodium chloride and 95% distilled water solution, with pH range of 6.5-7.2 and spray chamber temperature of $35\pm^{1.1}_{1.7}$ °C for different exposure durations so that different corrosion levels were obtained. Pitting was initiated on the specimens after 10, 20, and 30 days corrosion level, and which became progressively more severe versus time. After salt-spray exposure, the specimens were washed with clean water, according to ASTM G 1-72 procedure, in order to remove any remaining salt deposits from their surface and then dried.

$BSt500_s$ steel in maximum permissible values of the final product contains C = 0.240%, P = 0.055%, S = 0.055%, and N = 0.013%. The Material Yield stress is ≥500 (MPa), the Tensile strength ≥550 (MPa), the Elastic modulus 200 (GPa), and the (%) Elongation (after breaking) ≥12.

2.2 Mass Loss

The steel corrosion level was measured as the percentage of the difference between initial and final masses before and after corrosion. The relationship between the remaining mass and corrosion duration is shown in Table 1.

The steel specimens were cut and prepared in cross and transverse sections, shown in Fig. 1, in order to examine the surface thickness variation of the martensitic layer, which appears to be higher in the location of the ribs and lower in between them and also the influence of the salt-spray corrosion. The preparation included sectioning/resin immersion/grinding/ and polishing. Nital was used for the chemical etching.

From Fig. 2 and 3, it may be seen that the average thickness of the martensitic layer for noncorroded steel was approximately 0.95 mm while the corresponding thickness after 90 days corrosion was 0.40 mm. Table 2 shows the martensitic layers thickness in the cross and transverse sections of the specimens.

The corrosion process created notches and cavities in the outer surface of the specimens as shown in Fig. 3, with depth measured approximately 0.40 mm after 90 days corrosion level. The roughness and crack formation in the outer surface is mostly responsible for the material mechanical properties and ductility degradation.

In reinforced concrete structures and when steel corrosion in statically critical areas where recycling has devaluated the concrete then the notches and cavities may become critical for the structural integrity.

Table 1 Mass loss and remaining diameter at different corrosion levels

Exposure to salt-spray corrosion environment							
Exposure time (days)	0	10	20	30	45	60	90
Mass loss (%)	0	1.35	2.00	3.03	4.89	6.65	10.40
Diameter (mm)	12.00	11.92	11.88	11.82	11.70	11.59	11.36

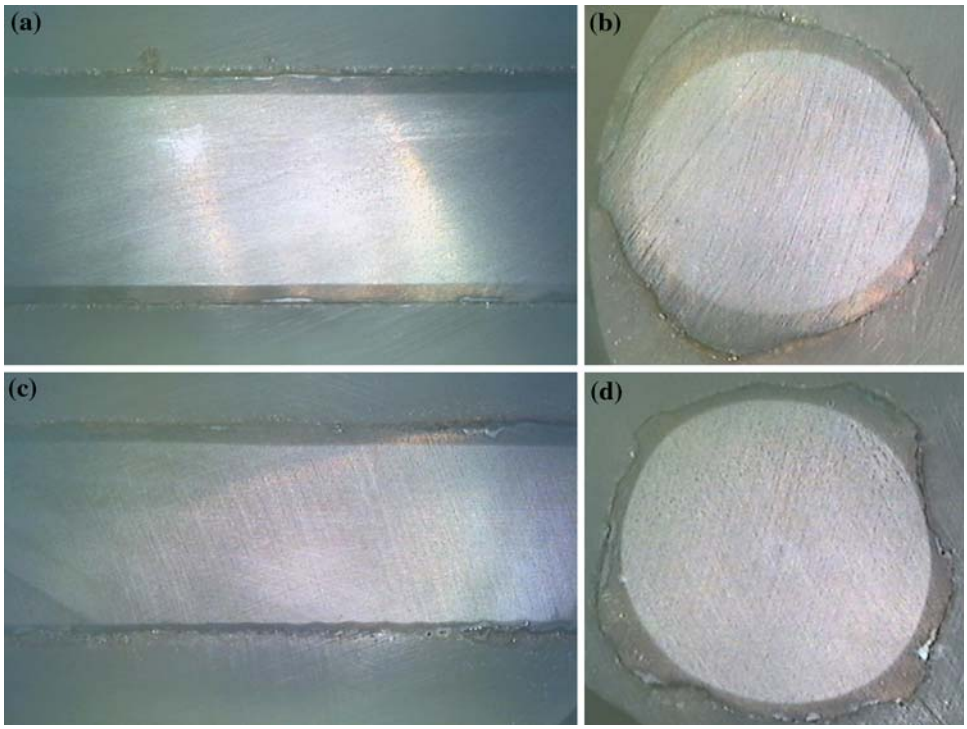

Fig. 1 Stereoscopic images. (a) Transverse section of noncorroded specimen; (b) Cross section of noncorroded specimen; (c) Transverse section of 90 days corroded specimen; (d) Cross section of 90 days corroded specimen

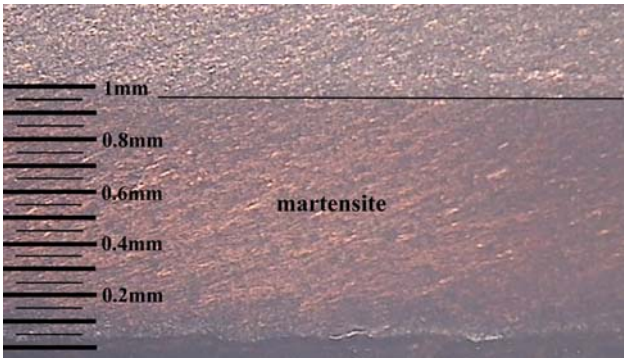

Fig. 2 Martensitic layer thickness of noncorroded specimen, transverse section

The area A_s used in the calculation of the fatigue stress was determined according to DIN 488-3 specification as

$$A_s = \frac{1.274 \times M_f}{l} \quad \text{(Eq 1)}$$

where M_f is the final mass and l is the bar length. The corrosion process created pitting, cavities, and notches on the steel surface and especially the rib bases, which became more severe as the corrosion level increased. The pitting developed on the steel surfaces even after removal of the rust is shown in the stereoscopic images of Fig. 3. The relatively large pits at 90 days of salt-spray exposure suggest that these are the active sites at which corrosion is primarily taking place. Pitting was initiated at the reinforcement veins of the steel bars and progressed towards the intermediate space. The gradual

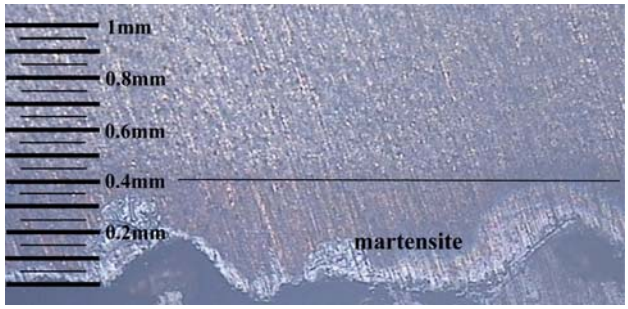

Fig. 3 Martensitic layer thickness of 90 days corroded specimen, transverse section

Table 2 Martensitic layer thickness

	Cross sections		Transverse sections	
Specimen	**Min, mm**	**Max, mm**	**Min, mm**	**Max, mm**
Noncorroded	0.8	1.5	0.7	1.2
Corroded for 90 days	0.35	0.9	0.12	0.7

decrease of the strength characteristics is related to the mass loss and in particular on the reduction of the thickness of the more resistive martensitic outer layer.

2.3 Stereoscopic Images, SEM

Figure 4-10 show Scanning Electron Microscopic observations of the corrosion of $BSt500_s$ tempcore steel. The presence of air in the iron/water interface is detrimental to the corrosion

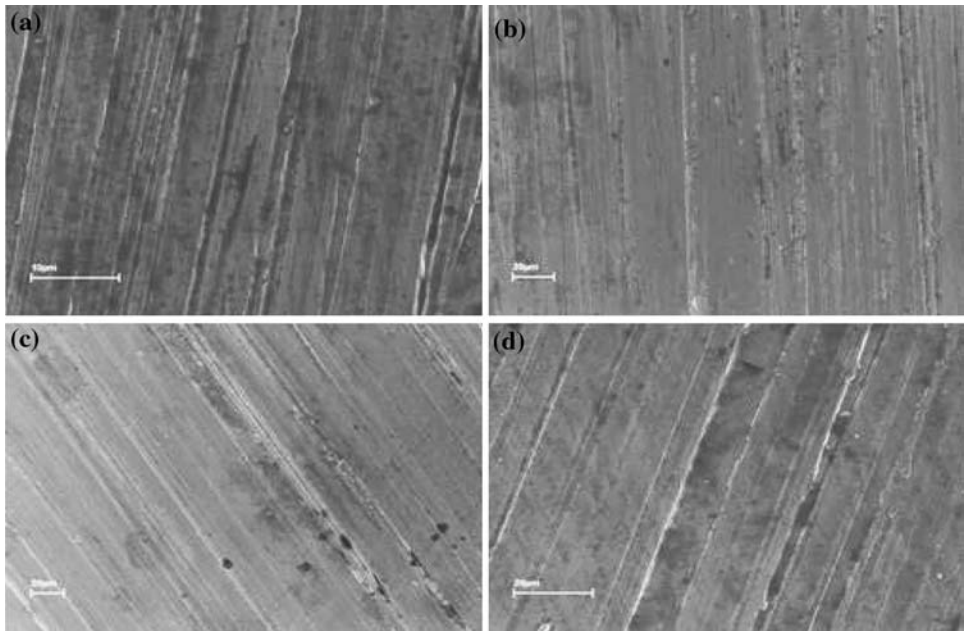

Fig. 4 Morphology of cross sections of $BSt500_s$ noncorroded steel

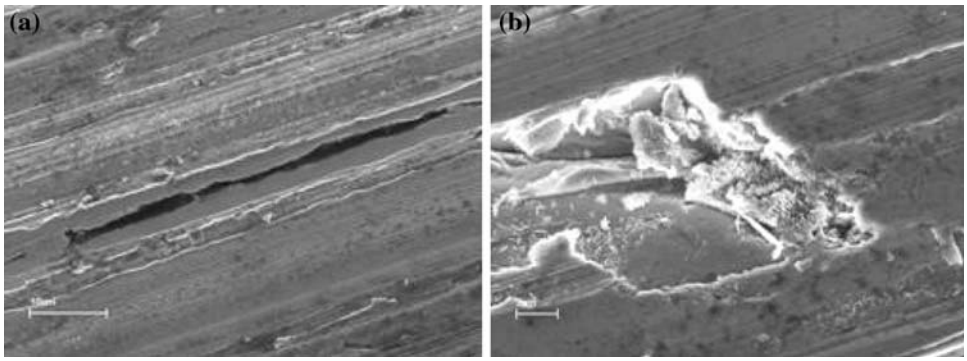

Fig. 5 Cross sections of $BSt500_s$ steel corroded for 45 days

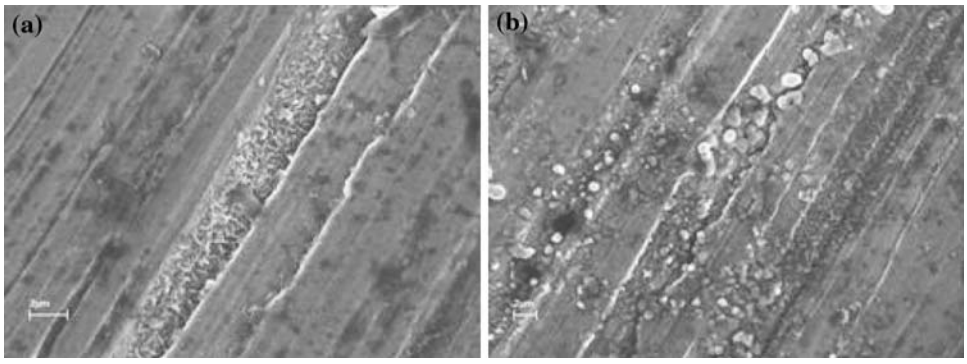

Fig. 6 Cross sections of $BSt500_s$ steel corroded for 45 days

process which is responsible for the deterioration of steel bars used in concrete. Tests conducted in salt-spray chambers are most suitable for demonstrating the corrosion process which is accelerated by the presence of chloride ions.

In Fig. 4(a) and (b) the morphology of cross sections of $BSt500_s$ steel specimens is shown and as may be seen the surface shows only polishing lines. Transverse sections are shown in Fig. 4(c) and (d).

Following 45 days exposure in a salt-spray chamber, the material damage is shown in cross section in Fig. 5(a) and (b). Severe damage may be observed from the deterioration of the surface, the development of crevices and corrosion products in

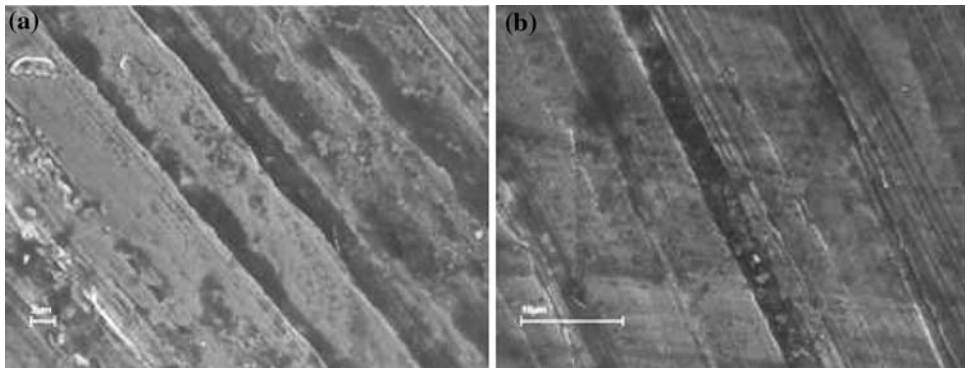

Fig. 7 Transverse sections of $BSt500_s$ steel corroded for 45 days

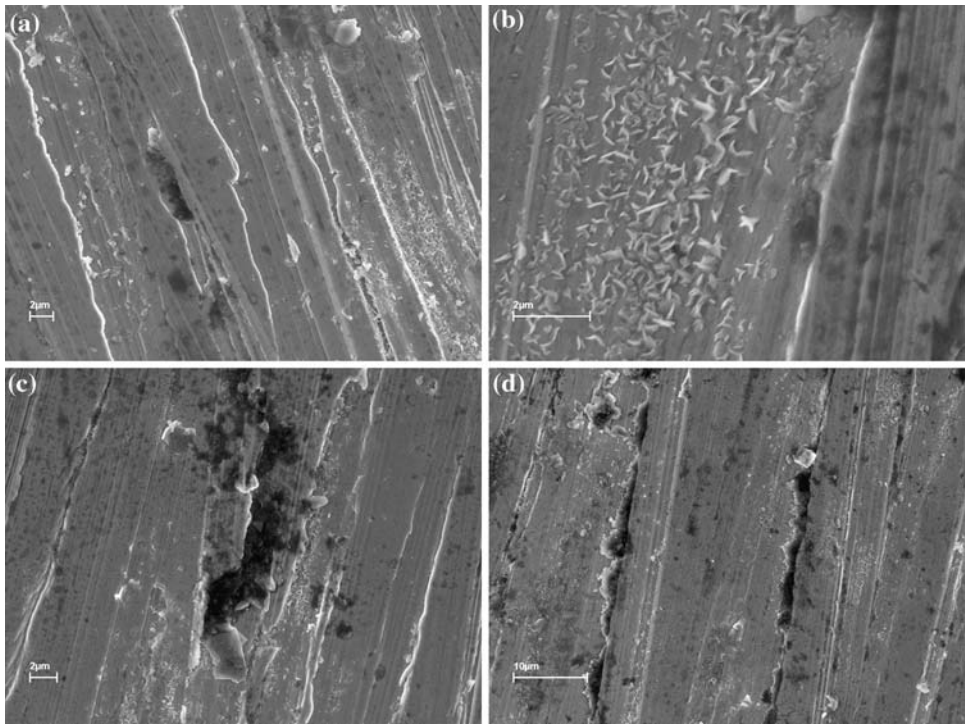

Fig. 8 Cross sections of $BSt500_s$ steel corroded for 90 days

the form of submicron plate-like crystallites shown in Fig. 5(b).

The plate-like crystallites form into the crevices developed on the damaged surface shown in Fig. 6(a) while at the same time, spherulitic formations of corrosion products formed at the sites where the surface appears to be damaged.

The morphology of the longitudinal section of the specimens exposed in the salt-spray chamber for 45 days, shown in Fig. 7(a) and (b), revealed the formation of tubules in which mass loss has apparently taken place, due to corrosion. From the morphology of the damage, serious consequences of the material strength may be anticipated.

Prolonged exposure in the salt-spray chamber for 90 days, revealed enhanced damage. The morphology of the cross sections of the steel specimens shown in Fig. 8 revealed the complete damage of the surface layer of steel with submicron plate-like corrosion products.

Figure 9 shows formation of channels, similar to those found in the case of the 45 days exposure in the salt-spray chamber. As may be seen, in addition to the pronounced channel formations, Fig. 9(c) and (d), the sections were ''perforated'' with dispersed pits shown in Fig. 9(b) and interrupted by formations of corrosion by-products as shown in Fig. 9(a).

Examination of the transverse cross sections revealed the significant recession of the surface of the specimens as shown in Fig. 10, which may well account for the reduced strength measured at the 90 days of exposure in the corrosive atmosphere of the salt-spray chamber.

2.4 Low Cycle Fatigue

The effect of corrosion on low cycle fatigue behavior of $BSt500_s$ tempcore steel under earthquake conditions was

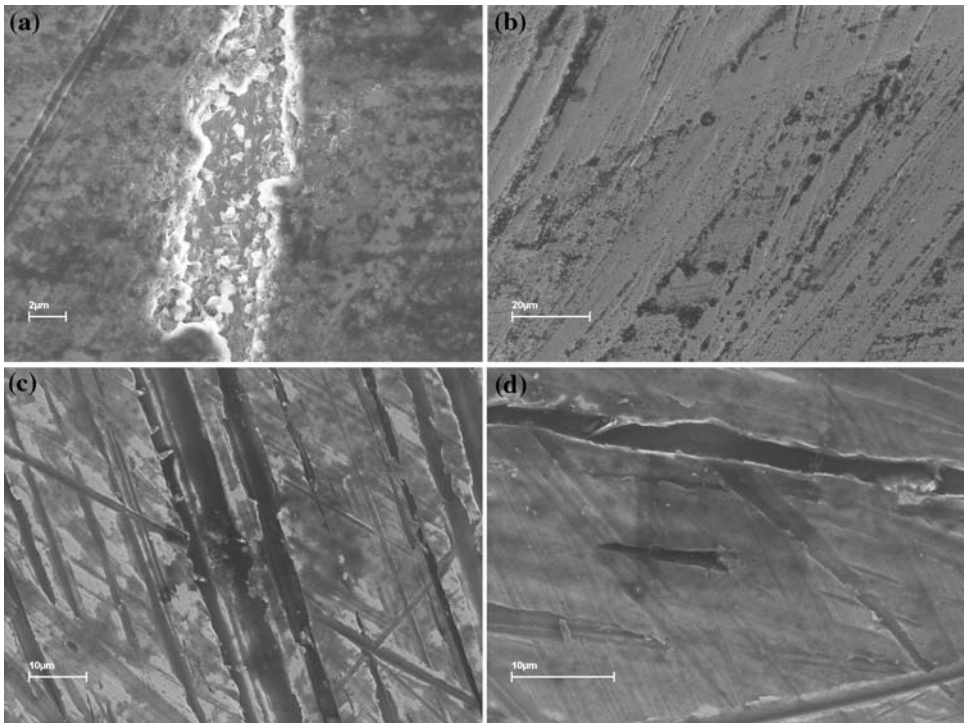

Fig. 9 Transverse sections of $BSt500_s$ Tempcore steel corroded for 90 days

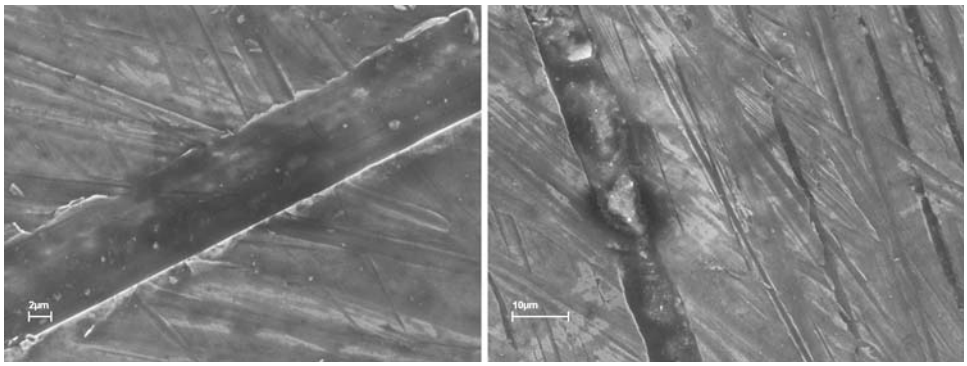

Fig. 10 Transverse sections of $BSt500_s$ steel corroded for 90 days

investigated experimentally, under uniaxial sinusoidal loads of 1 Hz frequency and constant strain amplitude of ±1, 2.5 and 4% after being exposed to accelerated salt-spray corrosion for different durations. Sixty-three low cycle fatigue tests were conducted, three for each corrosion level at 0, 10, 20, 30, 45, 60, and 90 days and for ±1, 2.5, and 4% strain levels.

The 12 mm diameter specimens were cut at 172 mm length and the free length between grips was set at an empirical value of $6 \times 12 = 72$ mm, since this is approximately the free bar length between stirrups in critical regions of columns in earthquake prone areas. In order to avoid misleading results, the specimens' geometry remained unchanged contrary to ASTM E606 standards for strain-controlled fatigue testing. Modification in the geometry, in order to comply with the ASTM E606 standards for strain-controlled fatigue testing, would alter the nature of the material thus giving misleading results in the LCF tests. The analytical expression for total strain is given by (Ref 12)

$$\frac{\Delta\varepsilon_t}{2} = \frac{\Delta\varepsilon_e}{2} + \frac{\Delta\varepsilon_p}{2} = \frac{\sigma_f'}{E}(2N)^b + \varepsilon_f'(2N)^c \quad \text{(Eq 2)}$$

where: $\Delta\varepsilon_t$, $\Delta\varepsilon_e$, and $\Delta\varepsilon_p$ are the total, elastic, and plastic strain amplitudes, respectively, ε_f' and c are the fatigue ductility coefficient and exponent, respectively, σ_f' and b are the fatigue strength coefficient and exponent, respectively, and E is the modulus of elasticity. Knowing the significance of the plastic strain to the life expectancy of steel reinforcement Fig. 11 shows representative experimental typical hysteresis loops for LCF and as it can be seen that corrosion and applied strain levels are the predominant factors to material-inflicted damage. Therefore for 1% applied strain, the plastic deformation ($\Delta\varepsilon_p$) in the noncorroded case occupies approximately 25% of the width of the loop while at 90 days corrosion level, it increases to approximately 32%. For 2.5% applied strain, the corresponding values for plastic

deformation ($\Delta\varepsilon_p$) in the noncorroded case and 90 days corrosion are approximately 63% and 69% of the width of the loop. For 4% applied strain, the corresponding values for plastic deformation ($\Delta\varepsilon_p$) in the noncorroded case and 90 days corrosion are approximately 75% and 80% of the width of the loop.

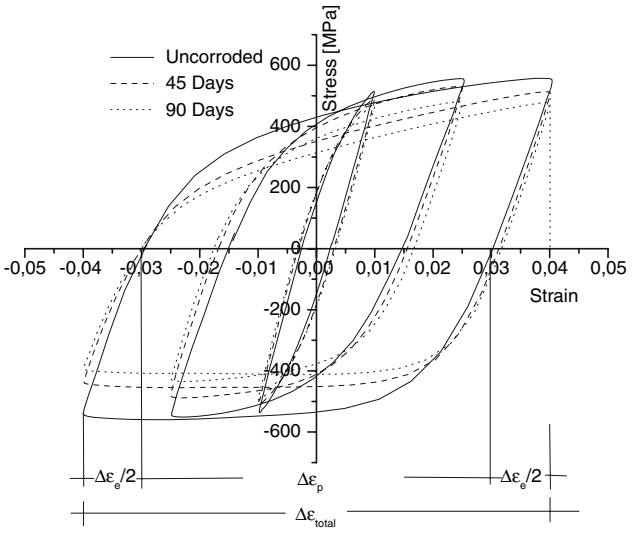

Fig. 11 Typical LCF stress-strain diagrams, at ±1, 2.5, and 4% applied strain, showing hysteresis loops for initial, middle, and final cycles for steel corroded at various levels

The total dissipated energy density was evaluated as the sum of the areas formed within the hysteresis loops. This measures the capacity of the material to absorb energy during seismic activity. Even though random noncorroded and corroded specimens are represented, it is clearly shown that plastic deformation ($\Delta\varepsilon_p$) is predominant and as the applied strain increases the plastic deformation, $\Delta\varepsilon_p$, also increases. For 1% strain level the degree of corrosion was found to have a significant effect on the number of cycles to failure, but for 2.5% and 4% strain levels, corrosion appears to be of secondary nature. As shown in Fig. 12 and Table 3, an increase in exposure time results in reduction of the life expectancy.

It is finally apparent that the reduction of the useful life of steel is closely related to the loading history, the width of the subjected strain and the imposed corrosion level.

Since the LCF tests were performed at constant strain amplitude, the maximum resisting force exerted by the specimens for each cycle is gradually reduced. Figure 11 shows a drop in the force-bearing capacity versus time. Furthermore, an overall reduction of the applied force is observed for the pre- and post-corroded specimens which were expected since the cross-sectional area was reduced with advancing corrosion. The reinforcing steel used in structures is

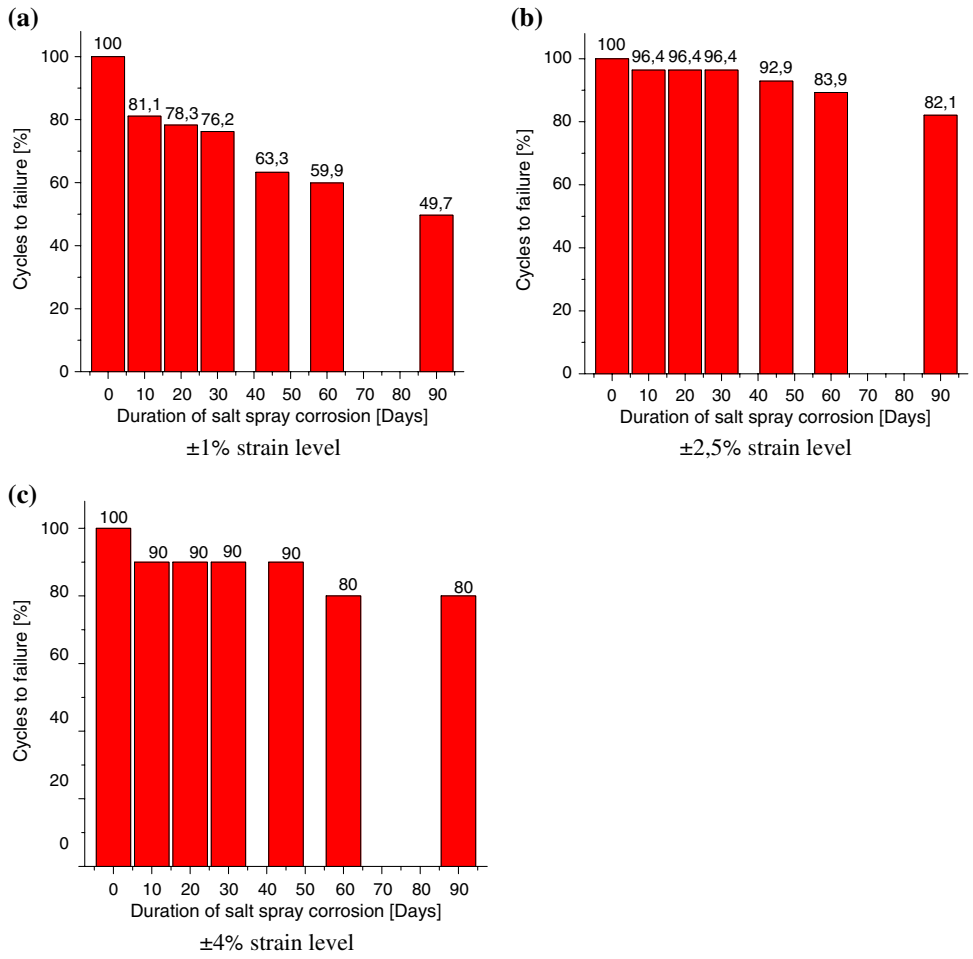

Fig. 12 Effect of corrosion on life expectancy

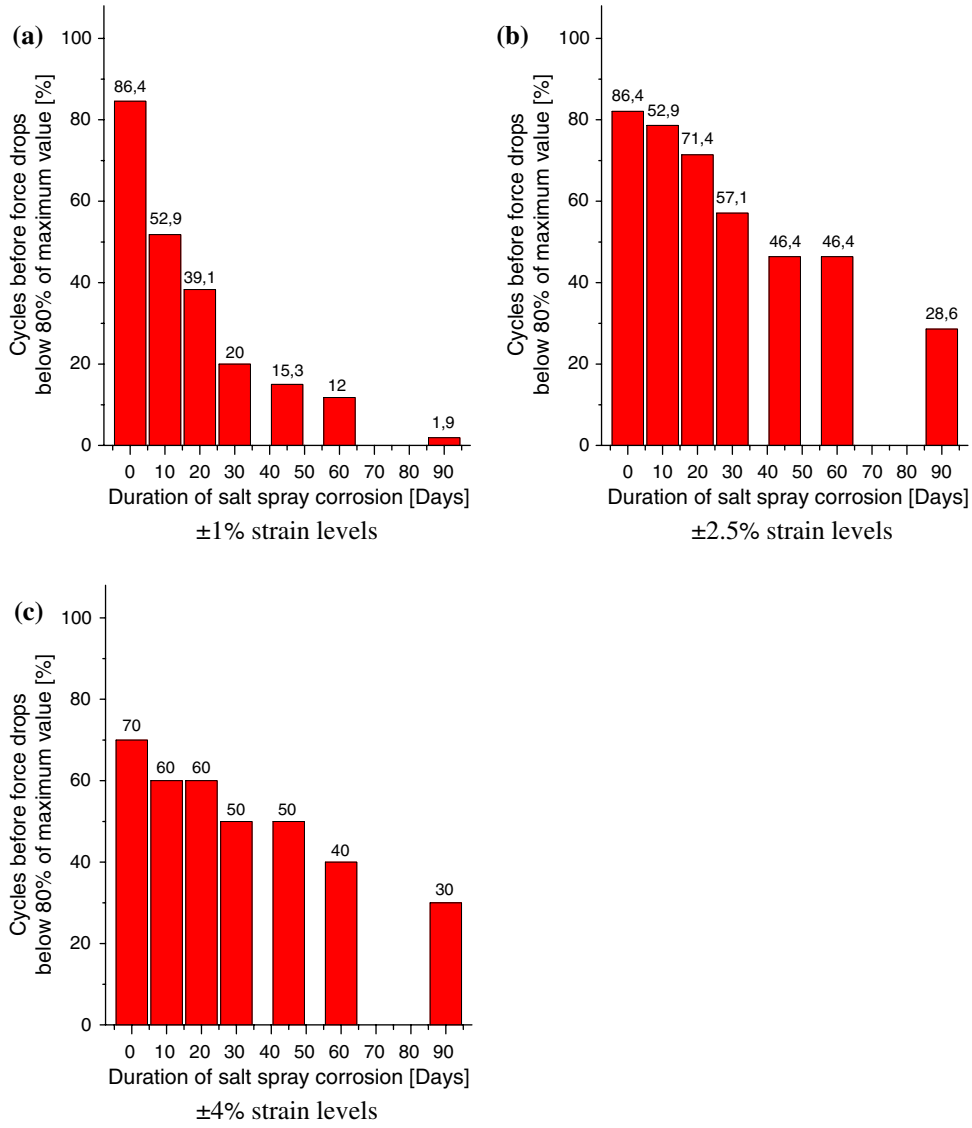

Fig. 13 Life expectancy of steel before the load capacity drops below 80% of the maximum value

Table 3 Effect of corrosion on life expectancy

Cycles to failure at different strain levels			
	Strain level		
Duration of salt-spray corrosion	±1%	±2.5%	±4%
Noncorroded	529	28	10
10 days	429	27	9
20 days	414	27	9
30 days	403	27	9
45 days	335	26	9
60 days	317	25	8
90 days	263	23	8

Table 4 Life expectancy of steel before load capacity drops below 80% of the maximum value

	Strain level		
Duration of salt-spray corrosion	±1%	±2.5%	±4%
Noncorroded	457	23	7
10 days	280	22	6
20 days	207	20	6
30 days	108	16	5
45 days	81	13	5
60 days	64	13	4
90 days	10	8	3

expected to carry a constant load throughout its service life since this remains fairly constant over time. As may be seen from Fig. 13 for a threshold of 80% of the maximum force of the noncorroded material and as the corrosion level increases, the remaining life for which the material can support this force is greatly reduced. Table 4 shows the specimens' failure behavior versus salt-spray duration, total dissipated energy density and cycles to failure before and after the 80% threshold

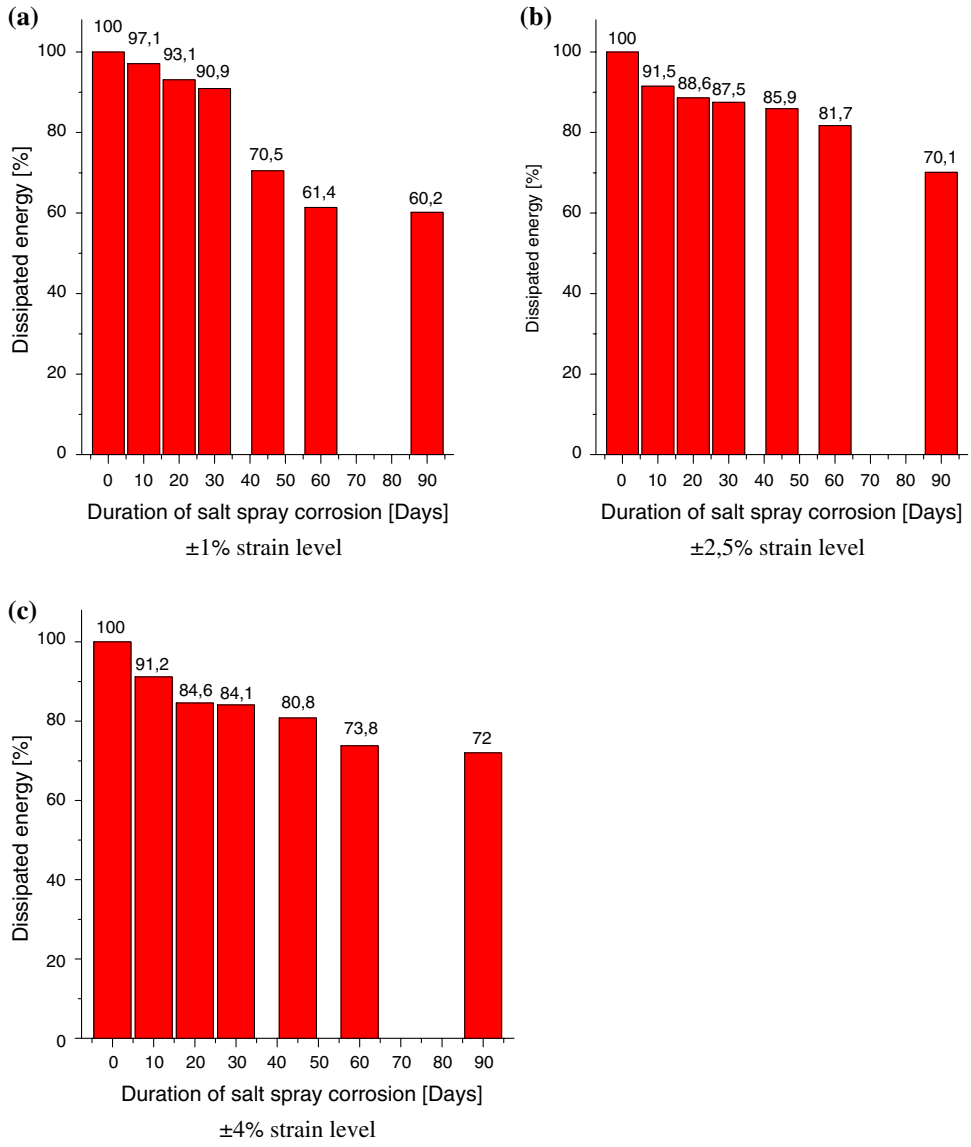

Fig. 14 Effect of corrosion duration on dissipated energy

load limit. As corrosion level increases, the number of cycles to failure decreases.

Figure 14 summarizes the effect of corrosion on the total dissipated energy for different strain levels. The observed appreciable reduction may represent a serious problem for the safety of constructions in seismically active areas. If U is the available energy density of the noncorroded material, and U_{90} is the available energy density of the 90 days corroded material, then it is worth noting that the ratio U/U_{90} for strain levels ±1, ±2.5, and ±4% remains fairly constant at 1.66, 1.43, and 1.39 respectively. It is certain that a further strain level increase will result in even smaller ratios with tendency to reach a constant value near unity, the value of which will depend on the level of embrittlement and stress concentration.

Table 5 summarizes the dissipated energy versus life expectancy for ±1, ±2.5, and ±4% strain levels and different corrosion durations.

Figure 15 shows the influence of corrosion on the mass loss and the decrease in life expectancy.

Table 5 The impact of corrosion duration on dissipated energy

	Strain level		
Duration of salt-spray corrosion	**±1%**	**±2.5%**	**±4%**
Uncorroded	2329	753	454
10 days	2262	689	414
20 days	2168	667	384
30 days	2117	659	382
45 days	1643	647	367
60 days	1430	615	335
90 days	1403	528	327

3. Summary of Results

An experimental investigation was conducted in order to study the impact of corrosion on the mass loss, mechanical

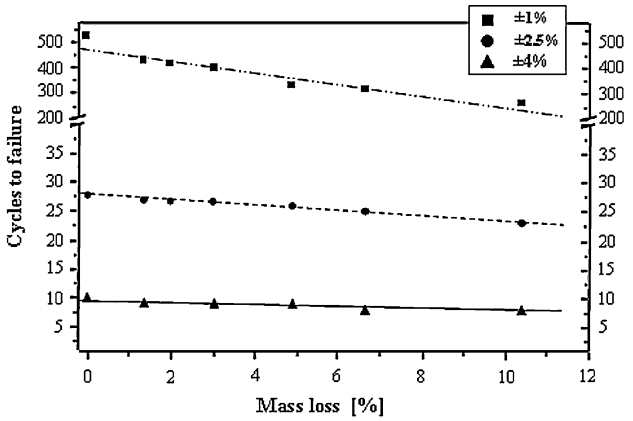

Fig. 15 Effect of corrosion on mass loss and life expectancy

properties, and fatigue life of 12 mm diameter, artificially corroded $BSt500_s$ reinforcing steel. Sodium chloride corrosion and LCF simulate satisfactorily the natural corrosion process and seismic loading. The results indicated a correlation between the load-bearing ability and life expectancy under LCF. Furthermore a reduction of the dissipated energy was noticeable, which is also confirmed by the gradually occurring embrittlement observed in the SEM photographs, caused by corrosion of the steel bars. The main degradation factors, corrosion and LCF are time-dependent, thus making the reliability of $BSt500_s$ steel a function of time as well.

Figure 1 shows stereoscopic images of the transverse and cross sections of noncorroded and corroded for 90 days specimens. The serious impairment inflicted on the exterior martensitic layer can be observed which is a source of high stress concentration points for both tension and compression.

Figure 2 and 3 show the martensitic layer thickness of noncorroded and 90 days corroded specimens. The general reduction of the cross-sectional area and the creation of surface abnormalities that constitute sources of high stress concentration points are responsible for the drop in the strength properties and life duration under LCF.

The corrosion process created notches and cavities in the outer surface of the specimens as shown in Fig. 3, with depth measured approximately 0.40 mm after 90 days corrosion level. The martensitic layer thickness for noncorroded steel was approximately 0.95 mm.

Figure 4-10 shows the morphology of cross and transverse sections of $BSt500_s$ of noncorroded and corroded for 45 and 90 days steel. Channel formation is evident at 45 days corrosion while at 90 days these defects are more evident.

Figure 11 shows a typical LCF stress-strain diagrams, at ±1, 2.5, and 4% applied strain, showing hysteresis loops for initial, middle, and final cycles for steel corroded at various levels.

Figure 12 shows the effect of corrosion on life expectancy of steel. For 1% strain level, the degree of corrosion was found to have a significant effect on the cycles to failure, but for 2.5% and 4% strain levels corrosion appears to be of secondary nature. An increase in exposure time results in reduction of the life expectancy. It is also indicated that for low strain levels of ±1%, a greater service life reduction occurs (50.3% for 90 days of accelerated salt-spray corrosion) in comparison with ±2.5% and ±4%, where the reduction observed seems to be stable at ≤ 20%.

Figure 13 shows that for a threshold of 80% of the maximum force of the noncorroded material and as the corrosion level increases, the remaining life for which the material can support this force is greatly reduced. As corrosion level increases, the life expectancy of the material decreases.

Figure 14 shows that as strain levels increase, corrosion has a smaller impact on the dissipated energy.

Figure 15 shows the influence of mass loss due to corrosion on the life expectancy of steel, which decreases linearly. For the 1% strain level, it appears that the rate of reduction is much greater than in the 2.5% and 4% levels.

Up to now the seismic codes for designing new structures and for evaluating the structural integrity of existing ones, was based on calculations of the seismic loads via a spectrum of accelerations described and were adopted by the Federal Emergency Management Agency (FEMA-310) (Ref 24). Recently, the FEMA reevaluation provides that this design is based on calculations via a displacement spectrum (Direct displacement-based assessment or design). The threshold limits, however of the permissible displacements of these new codes are not fully representative or realistic since they do not anticipate the degradation of the mechanical properties of the steel reinforcement. Structural assessment of older buildings based on mathematical models (displacement-pushover method) may lead to unreliable and inaccurate results since the degradation of the material strength and ductility properties are not taken into consideration.

4. Conclusions

Steel used for concrete reinforcement is vulnerable to atmospheric sodium chloride corrosion and the testing conducted in this investigation has shown:

1. (a) A strong correlation between corrosion and mass loss for 10-90 days corrosion level of the order of 1.35-10.40%, respectively. The dependency of corrosion on mass loss and fatigue strength has an important practical interest. (b) Steel deterioration was initiated at the rib base and progression of corrosion induced further wear of the ribs, which after 90 days, corresponding to 10.40% mass loss, caused considerable reduction of the average height of the ribs and the martensitic layer thickness. (c) The SEM photographs for the 90 days corrosion samples show formation of channels, similar to those found in the case of the 45 days exposure in the salt-spray chamber. In addition to the pronounced channel formation the sections were "perforated" with dispersed pits shown and interrupted by formations of corrosion by-products.
2. Drastic reduction of the fatigue limit was observed due to wear of the exterior hard layer of martensite and drastic drop in the energy density. Stress concentration points were developed, localized at imperfections and especially in the pits and notches of the rib bases of the corroded steel, which were also justified by the SEM micrograph results. Progressive pitting accompanied by partial loss of the outer martensitic layer and formation of outer roughness were evident. These areas are considered critical for the formation of stress concentration points and responsible for the reduction of strength, elongation to fracture,

energy density, and fatigue life. Thus the increased corrosion reduced the useful life of steel.

3. Evaluation of the integrity of older structures using mathematical models (displacement-pushover method) and the properties of reference materials leads to overestimating and erroneous results since the degradation of the material strength and ductility properties are not taken into consideration.

References

1. J.P. Broomfield, *Corrosion of Steel in Concrete*. E & FN Spon, London, 1997, p 22
2. V.G. Papadakis, *Supplementary Cementing Materials in Concrete – Activity, Durability and Planning*. Danish Technological Institute Concrete Center, January 1999
3. R. Capozucca, Damage to Reinforcement Concrete due to Reinforcement Corrosion, *Constr. Build Mater.*, 1995, **9**(5), p 295–303
4. M.G. Alvarez and J.R. Galvele, The Mechanisms of Pitting of High Purity Iron in NaCl Solutions, *Corros. Sci.*, 1984, **24**, p 27–48
5. G.K. Glass and N.R. Buenfeld, Chloride-induced Corrosion of Steel in Concrete, *Prog. Struct. Eng. Mater.*, 2000, **2**(4), p 448–458
6. C. Fang, K. Lundgren, L. Chen, and C. Zhu, Corrosion Influence on Bond in Reinforced Concrete, *Cem. Concr. Res*, 2004, **34**(11), p 2159–2167
7. A. Ouglova, Y. Berthaud, M. François, and F. Foct, Mechanical Properties of an Iron Oxide Formed by Corrosion in Reinforced Concrete Structures, *Corros. Sci.*, 2006, **48**(12), p 3988–4000
8. A.A. Almusallam, A.S. Al-Gahtani, A.R. Aziz, and P. Rasheeduzzafar, Effect of Reinforcement Corrosion on Bond Strength, *J. Constr. Build. Mat.*, 1996, **10**(2), p 123–129
9. A.A. Almusallam, A.S. Al-Gahtani, A.R. Aziz, F.H. Dakhil, and P. Rasheeduzzafar, Effects of Reinforcement Corrosion on Flexural Behavior of Concrete Slabs, *J. Mat. Civil Eng.*, 1996, **8** (3), p 123–127
10. Ch.Alk. Apostolopoulos and D. Michalopoulos, The Effect of Corrosion on the Mass Loss and Low Cycle Fatigue of Reinforcing Steel, *JMEP*, 2006, **15**(6), p 742–749
11. J.P. Broomfield, *Corrosion of Steel in Concrete: Understanding, Investigation and Repair*. St. Edmundsbury Press Limited, Bury St. Edmunds, Suffolk, Great Britain, 1997
12. H.O. Fuchs and R.I. Stephens, *Metal Fatigue in Engineering*. John Wiley & sons Inc, USA, 1980, p 76–82
13. G.M. Sheng and S.H. Gong, Investigation of Low Cycle Fatigue Behaviour of Building Structural Steels Under Earthquake Loading, *Acta Metall. Sin. (English letters)*, 1997, **10**(1), p 51–55
14. T. Yoshaki, *Proceedings of Academical Lectures of JAS*. Tokyo, 1983, p 606
15. H. Shigeru, Research Report "Retrofitting of Reinforced Concrete Moment Resisting Frames" supervised by Park, R and Tanaka, H. ISSN0110-3326, August 1995
16. Z.P. Bazant, Physical Model for Steel Corrosion in Concrete Sea Structures-theory, *J. Struct. Div.*, 1979, **105**, p 1137–1153
17. J. Cairns, G.A. Plizzari, Y. Du, D.W. Law, and C. Franzoni, Mechanical Properties of Corrosion-Damaged Reinforcement Title No. 102-M29, *ACI Mater. J. Technical Paper*, 2005, **102**(4), p 256–264
18. X. Wang and X. Liu, Bond Strength Modelling for Corroded Reinforcements, *Constr. Build. Mater.*, 2006, **20**, p 177–186
19. J.G. Cabrera, Deterioration of concrete due to reinforcement steel corrosion, *Cement and Concrete Composite*, 1996, **18** (l), p 47–59
20. C.A. Apostolopoulos and M.P. Papadopoulos, Tensile and Low Cycle Fatigue Behavior of Corroded Reinforcing Steel Bars S400, *J. Constr. Build. Mater.*, 2007, **21**, p 855–864
21. Ch.Alk. Apostolopoulos, Mechanical Behavior of Corroded Reinforcing Steel Bars $S500_s$ Tempcore Under Low Cycle Fatigue, *J. Constr. Build. Mater.*, 2007, **21**, p 1447–1456
22. Ch.Alk. Apostolopoulos and D. Michalopoulos, Corrosion of Reinforcing Steel and Low Cycle Fatigue Behaviour, *Mater. Corros.*, 2007, **58**(6), p 1–10
23. M.G. Fontana, *Corr. Eng.*, 1987 (New York), McGraw-Hill, 3rd ed
24. FEMA-310, *Handbook for the Seismic Evaluation of Buildings*, A Prestandard, Prepared by the American Society of Civil Engineers for the Federal Emergency Management Agency, Washington, DC, 1998